유한요소법을 이용하여 확장기때 압력에 따른 심실심근의 응력 해석

한 근조*, 김 상현**, 신 정욱***
* 동아대학교 기계공학과
** 연세대학교 의용공학과
*** 인제대학교 의용공학과

Stress analysis of ventricular myocarda according to heart pressure in diastole using finite element method

Geun Jo Han*, Sang Hyun Kim**, Jung Woog Shin***
*Dept. of Mech. Eng. Dong-A. Univ.
**Dept. of Biomed. Eng. Younsei. Univ.
***Dept. of Biomed. Eng. Inje. Univ.

ABSTRACT

In order to study the shape and dimensions of heart, the procedures to reconstruct a three dimensional left ventricular geometry from two dimensional echocardiographic images is studied including the coordinate transformation, curve fitting and interpolation utilizing three dimensional position registration arm.

Nonlinear material property of the left ventricular myocardium was obtained by finite element method performed on the reconstructed geometry and optimization techniques which compare the computer predicted 3D deformation with the experimentally determined deformation. Afterwards using the obtained nonlinear material propertry the stress distribution related with oxyzen consumption rate was analyzed.

1. INTRODUCTION

A number of attempts have been made to analyze the mechanical behavior of the left ventrical which is closely related with the cardiac performance. Several of these studies have concentrated on the diastolic performance since abnormalities in diastolic function have been suggested to be precursor to systolic dysfunction. The diastolic function is usuallay evaluated by the left ventricular pressure-volume (P-V) curve. Attempts have also been made to compute the myocardial stress distribution since the underlying myocardial oxyzen demand is colsely related with the level of stress [1)2)]. For these investigations the study of the material properties of the myocardium during passive expansion such as Young's modulus and Poisson's ratio is essential. Finite element technique was used on the dimensional reconstructed (3D) geometries[3)-6)] of the left ventricle (LV) to assess the material properties of the myocardium.

In order to determine the nonlinear material[7)-11)] property of the left ventricular myocardium, a finite element analysis was performed on the reconstructed geometry. The nonlinear analysis was implemented by way of a stepwise linear analysis. The material properties of each step within a diastole are obtained by an optimization technique which compares the computer predicted 3D deformation with the experimentally determined deformation and the optimized elastic modulus is computed such that an error function representing the total difference is minimized. These optimized elastic moduli and the pressure increments obtained from the experimental measurements are used to analyse the stress in LV and RV geometry.

2. ECHOCARDIOGRAPHIC RECORDING

From the pressure recording, an interval where discrete pressure increase was observed in diastole was located and divided into three or four small intervals. With the measurement of the pressure increments which would be applied as pressure loads on the reconsturcted geometry, the points corresponding to the dividing points in pressure recording were sought on the ECG used as time referecne.

Cross-sectional echocardiographic images frozen at each dividing points of ECG were traced from the video monitor screen and superposed onto transparent sheets.

3. THREE DIMENSIONAL RECONSTRUCTION

3.1 Digitization of 2D images

The recorded images on the video tape are displayed and frozen in order to trace the endocardial and epicardial borders on transparent papers at various times in diastole. These traced echocardiographic images are digitized by a image processor connected to a computer or a Hewlett-Packard digitizer connected to a Prime computer. In each frame the LV epicardial and endocardial contrours are manually traced using the joystick hooked up to the image processor. The 2D LV cross-section image contours are converted to a discrete number of data points which are denoted by the x and y coordinates on the digitizer local coordinate system.

3.2 Coordinate transformation

The coordinates of the data points are digitized with respect to the local coordinate axes of the digitizer. In order to get the coordinates of those point with respect to the global coordinate system fixed in the experiment table, the coordinate transformation should be performed starting from the digitizer to the table via the transducer and the 3D arm by writing reconstruction program.

3.3 Nodal points

For the smooth surface of the epicardium and the endocardium reconstructed by this program, curve fitting and interpolation techniques are employed between the digitized points on each SAX. Therefore some points should be picked up according to the specified total number of the points on each contour. These selected points are refered to as 'nodal points' which are the key points in reconstructing the heart.

3.4 Curve fittings and interpolation

The process of curve fitting and interpolation on

the points are required because SAX's are neither parallel each other nor uniformly spaced and the total number of sections for finite element mesh generation may not always agree with the actual number of input SAX.

It is performed on the nodal points lying on the same long axis cross-section (LAX), i.e. the intersections of the contour and the same ith circular grid on each SAX.

4. OPTIMIZATION

The execution of the finite element analysis yields the displacements of each nodes as well as the stress and strain of each element and reaction forces on the constrained nodes. The deformed geometry predicted by the FEM is compared with the reconstructed geometry from the echocardiographic images at the next time interval, and modified by the optimized elastic modulus to have the two geometries match as closely as possible. Therefore there may be various ways of comparison and reduction of the mismatch. For most cases, the difference between the calculated displacements and the experimentally obtained displacements of each nodal points has to be utilized.

5. RESULTS AND DISCUSSION

Results of four experiments are plotted together in Fig. 1-2 with the pressure difference as applied loads as shown in Table 1. They were also obtained on the two cases where both the epicardium and endocardium or only the endocardium was considered in each optimization algorithm and compared. The displacement of endocardium is regarded to be more important since it shows a remarkable change whereas epicardium shows little change which is believed due to the pericardium constraining the movement of epicardium as observed in the echocardiac images.

When the geometric nonlinearity was included, the elastic modulus ranged from 3400 dyne/cm^2 (3.5 g/cm^2) at early diastole to 157000 dyne/cm^2 (160 g/cm^2) at around end diastole. The slope of the best fitting lines for the E-P plottings varied from 28.2 when the endocardium and the optimization algorithm 2 were used, to 41.6 when both contours and the optimization algorithm 1 were used.

From the experiments, the length of long, short axis and longitudinal axis were obtained and standardized to construct ellipsoid of major axis, 65mm, minor axis, 48.75mm and longitudinal axis, 55mm. The left ventricular myocardial thickness along the major axis was 12mm and the right ventricular thickness was 6mm.

To investigate the effect of nonlinear material property with the stepwise linear technique, we selected 9 loading cases. For the loading cases #1 to #5, an incremental pressure, 0.2mmHg obtained by dividing 1mmHg with 5 was applied and 5 different Young's moduli, 220 dyne/mm^2, 340 dyne/mm^2, 380 dyne/mm^2 were used, whose values were obtained from the E-P curve connecting two points (1 mmHg, 200 dyne/mm^2) and (2 mmHg, 400 dyne/mm^2) and dividing that line into 5 intervals. The mean values of Young's modulus for each interval were picked. In #6 and #7 cases, 1 mmHg was applied as a load and 200 dyne/mm^2, the starting value and 300 dyne/mm^2, the mean value between 200 dyne/mm^2 and 400 dyne/mm^2 was used as Young's modulus on the combined geometry of LV and RV. In #8 and #9 cases, all conditions are same exept that the simulation was implemented on LV geometry alone in order to understand the effect of RV geometry to LV.

When only the left ventricle model was analysed, its largest principal stress decreased along the endocardium from 0° to 90° in the counter-clockwise direction as shown in Fig. 3. It also decreased when plotted as in Fig. 5 from the top level to the bottom except that the stress curve for the top level is lower than those for the next two levels. It might result from the fact that the top level of the myocardium was cut through and open in the model even though the real ventricle should be closed and connected with atria. Hence, if the model was constructed so as to represent a whole heart composed of left and right ventricles as well as left and right artia the top level with largest dimensions compared with lower levels might have shown the highest stress distribution.

In other words, the deformation of the upper level above the top level, if the 4 chambers were modeled, would give bending effect to the top level. These trends were also found in the combined model of LV and RV as shown in Fig. 4(a)-(b), 6. But the magnitude of σ_1 for the combined geometry was quite larger than those for the LV only geometry, because the interventricular septum was affected by RV pressure as well as LV pressure. But the lateral side of left ventricular endorcardium showed slightly lower σ_1 distribution than the septal side of left ventricular endocardium. And the stress on the septal side of left ventricular epicardium on level #1-#4 was compressive but the absolute value of those decreased from the node of $\theta=0^0$ to the node of $\theta=45^0$ as shown in Fig. 7. Fig. 3(b), 4(b), 5, 6 showed the max. value of σ_1 occurred on the node of second level endocardium with $\theta=0^0$ and the min. value of σ_1 occurred on the node of same level epicardium with same θ.

In case #1 to #5 of stepwise linear study, the same incremental pressure 0.2 mmHg was applied on the geometry which was deformed geometry of previous stage. For example, in case #3, 0.2 mmHg was applied inside the LV and RV whose combined geometry was the deformed shape of #2 case. Hence, the coordinates of nodes in the initial geometry were obtained by adding those of #2 case initial geometry and the displacements.

We could observe that displacement of RV was quite larger than that of LV because the right ventricular wall thickness was thinner than LV thickness and that elliptical shape turned into round shape with almost same length of x and y axis in both LV and RV as shown in Fig. 8 (a)-(b).

According to Fig. 9 where the displacement was plotted based on the previous deformed shapes, D_{AP} change of case #5 in absolute value was 4.8 times larger than D_{SL} change. The most significant change was observed in D_{RL} because RV was deformed a lot more due to comparatively thin wall. In case #5 D_{RL} change was 2.7 times larger than D_{AP} change. All the dimensional change in absolute value increased from case #1 to #5 because the initial geometry got bigger although the applied load was same. The largest thickness change occurred in t_R. Next were t_L, t_S successively.

Comparing case #5 where 380 dyne/mm^2 and 0.2 mmHg were used for Young's modulus and pressure and case #6 where 200 dyne/mm^2 and 1 mmHg were used for the same parameters, we might expect that case #6 would bring out bigger displacement than case #5 because of the softer material property and higher pressure of case #6. But the result was reverse. From this fact we can conclude that the initial geometry size exhibited more significant effect on the displacement than Young's modulus and ventricular pressure.

We could observe the flattening tendency of septum in the combined geometry of LV and RV whereas the geometry of LV expanded sustaining almost the same eccentricity. So D_{SL} change increased in LV model and decreased in combined model. D_{AP} change increased in both models but D_{AP} of combined model changed more than that of LV model. Little difference in change of D_L was found in 2 models, which means RV geometry didn't give little effect in D_L change.

It could be found that t_S change in LV model was larger than that in combined model because LV model expanded freely but combined model couldn't expand as freely as LV model due to RV geometry and RV pressure. But t_L change was larger in combined model because LV lateral side could expand freely.

6. CONCLUSIONS

The three dimensional reconstruction technique from

the two dimensional echocardiographic images and the optimization algorithms in order to investigate the changing trend of elastic modulus depending on the ventricular pressure were described with the obtained nonlinear material property, stress distribution on the simulated geometry of LV and RV was implemented.

From the experiments and simulation following conclusions were obtained

1) When the geometric nonlinearity was included, the elastic modulus ranged from 3400 dyne/cm^2 (3.5 g/cm^2) at early diastole to 157000 dyne/cm^2 (160 g/cm^2) at around end diastole.

2) The maximum and minimum of σ_l in total geometry occured at nodes on the second level, intersection points of x-axis on the septal surface and endocardium or epicardium, respectively.

3) Lower level exhibited lower σ_l distribution except the top level which brought about the need for modeling the whole heart with two ventricles and two atria.

4) Node on anterior or posterior showed minimum σ_l along endocardium on a same level which was tensile in LV model and compressive in combined model because interventricular septum had the tendency to be flattened.

5) The most significant change of dimension in D_{RL}, which leaded to the same change in t_R, and shrinkage of D_{SL} resulted in the leftward shift of septum.

REFERENCES

(1) R. Beyar, and S. Sideman, Left ventricular mechanics related to the local distribution of oxygen demand throughout the wall, Circ. Res., 58, 664-677, 1986

(2) I.Mirsky, D.N.Ghista, H.Sandler, Cardiac Mechanics: Physiological, clinical, and mathematical considerations, John Wiley & Sons Inc., New York, 1974

(3) E.A. Geiser, D.J. Skorton, and D.A. Conetta, Quantification of left ventricular function from two-dimensional echocardiography, Am. J. Heart, 103, 903-910, 1982.

(4) K.R. Stickels, Wann, L.S An analysis of three-dimensional reconstructive echocardiography, Ultrasound in Med. & Biol., 10, 575-580. 1984.

(5) G.Joskowicz, M.Klicpera, P.Pachinger, Computer supported measurements of 2-D echocardiographic images, 1981 Computers in Cardiology, IEEE Computer Society, 13, 1981

(6) H.Sawada, J.Fujii, K.Kato, M.Onoe, Y.Kuno, Three dimensional reconstruction of the left ventricle from multiple cross sectional echocardiograms, Br. Heart J., 50:438, 1983

(7) S.A.Glantz, R.S.Kernoff, Muscle stiffness determined from canine left ventricular pressre-volume curves, Circ. Research, 37 : 787-794, 1975

(8) J.G. Pinto, Y.C. Fung, Mechanical properties of the heart muscle in the passive state, J.Biomechanics, 6:597-616, 1973

(9) J.D. Humphrey, R.K. Strumpf, and, F.C.P. Yin, Determination of a constitutive relation for passive myocardium:I. A new functional form, ASME J. of Biomechanical Engineering, 112, 333, 1990

(10) A.D. McCulloch, B.H. Smaill, and P.J. Hunter, Regional left ventricular epicardial deformation in the passive dog heart, Circ. Res., 64, 721, 1989.

(11) L.A. Taber, On a nonlinear theory for muscle shells: II. Application to the active left ventricle, ASME J. of Biomechanical Engineering, 113, 63, 1991.

Table 1 LV pressures and increments measured at several moments between early and late diastole.

Experiment	P_0	δP_1	P_1	δP_2	P_2	δP_3	P_3	δP_4	P_4
				(mmHg)					
#7	0.20	0.60	0.80	0.50	1.30	0.70	2.00		
#15	3.70	0.35	4.05	0.50	4.55	0.45	5.00	1.15	6.15
#16	3.90	0.50	4.40	0.90	5.30	1.30	6.60		
#17	1.42	0.83	2.25	0.92	3.17	1.42	4.58		

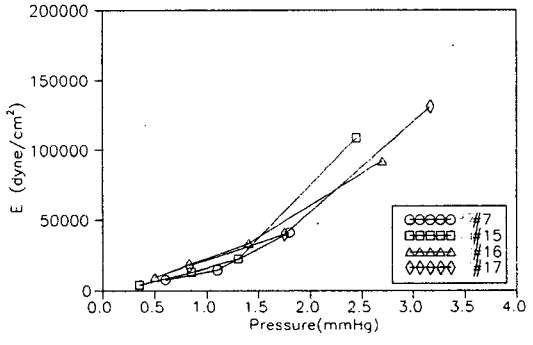

Fig. 1 Comparison of E-P curves of each experiment using optimization algorithm 1 and only endocardium

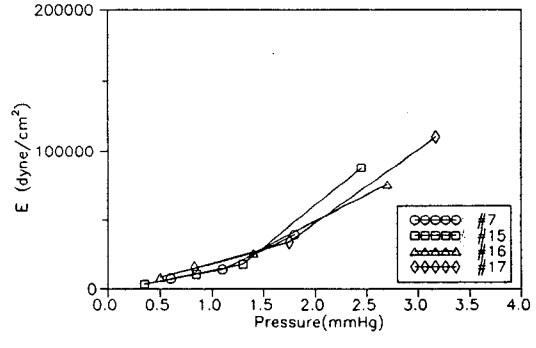

Fig. 2 Comparison of E-P curves of each experiment using optimization algorithm 2 and only endocardium

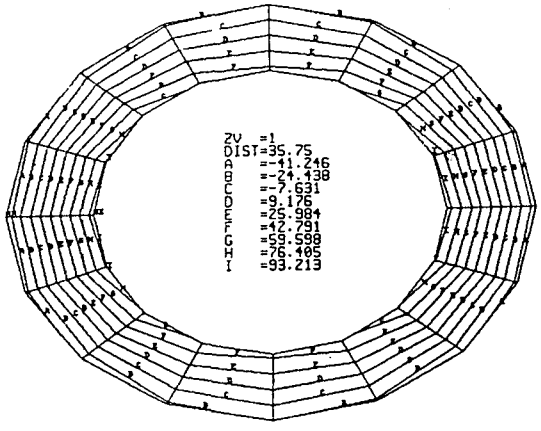

Fig. 3(a) σ_1 distribution on top level of left ventricle model

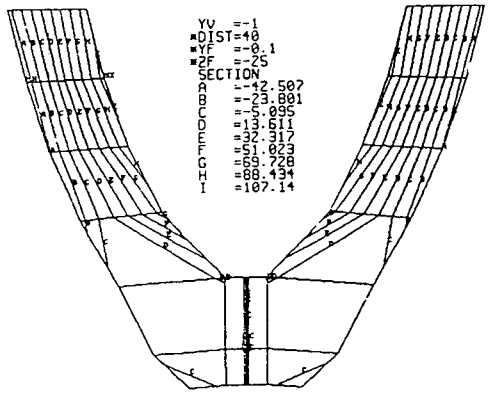

Fig. 3(b) σ_1 distribution on the middle section of left ventricle model cut along x-axis

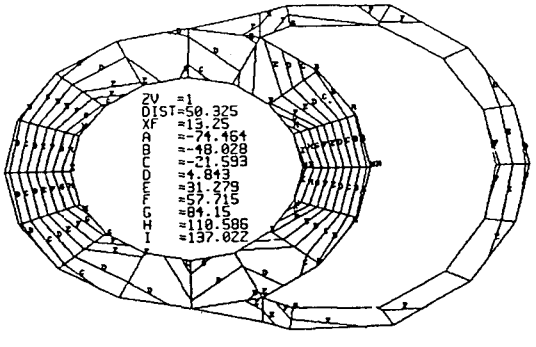

Fig. 4(a) σ_1 distribution on top level of combined model

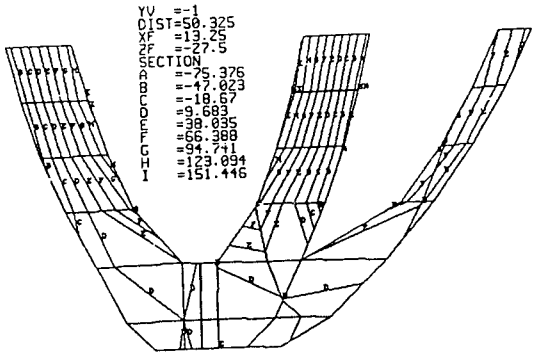

Fig. 4(b) σ_1 distribution on the middle section of combined model cut along x-axis

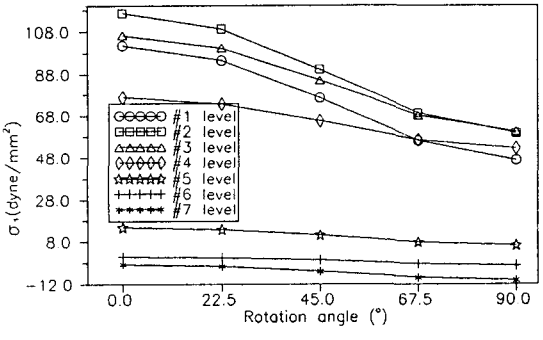

Fig. 5 Change of σ_1 depending on rotation angle θ on endocardium for 7 short axis levels of LV model

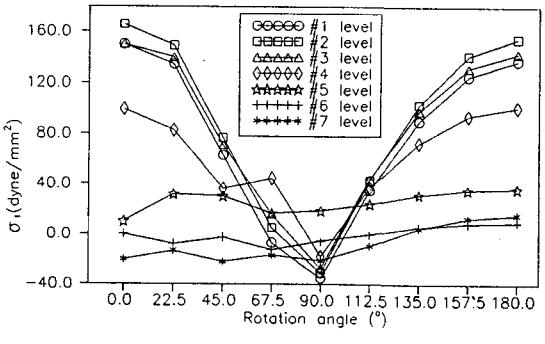

Fig. 6 Change of σ_1 depending on rotation angle θ on endocardium for 7 short axis levels of combined model

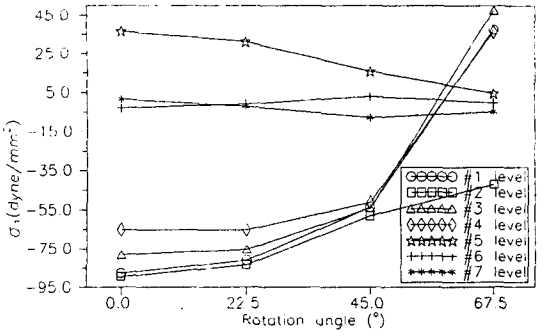

Fig. 7 Change of σ_1 depending on rotation angle θ on *epicardium for 7 short axis levels of combined* model

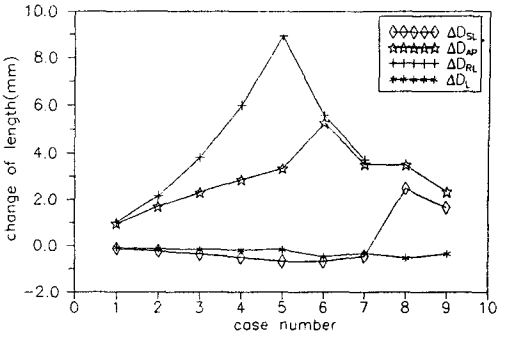

Fig. 9 Change of dimensions for 9 cases

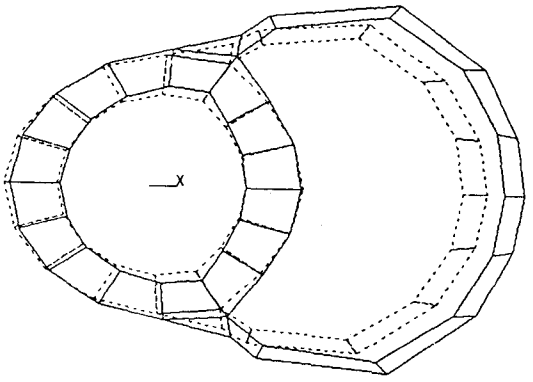

Fig. 8(a) Deformed shape (solid line) with initial geometry (dashed line) of top level for case #5

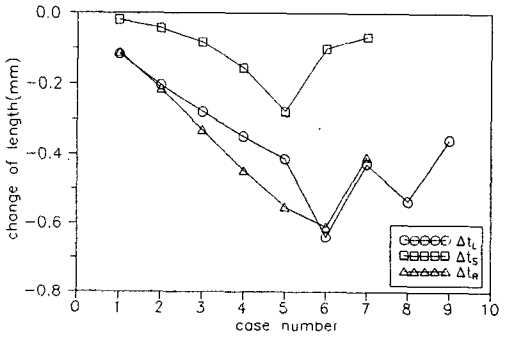

Fig. 10 Change of thickness for 9 cases

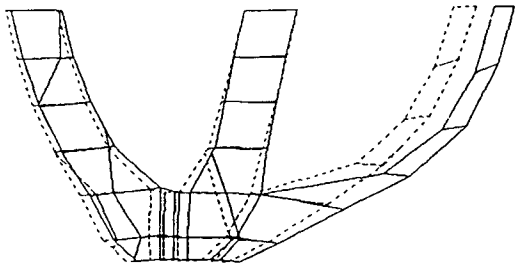

Fig. 8(b) Deformed shape (solid line) with initial geometry of middle section cut along x-axis for case #5